Article

Constructing bimetal, alloy, and compound-modified nitrogen-doped biomass-derived carbon from coconut shell as accelerants for boosting methane production in bioenergy system

Teng Ke[1], Sining Yun[1,2,*], Kaijun Wang[1], Tian Xing[1], Jiaoe Dang[1], Yongwei Zhang[1], Menglong Sun[1], Jinhang An[1], Lijianan Liu[1], Jiayu Liu[1]

[1]Functional Materials Laboratory (FML), School of Materials Science and Engineering, Xi'an University of Architecture and Technology, Xi'an 710055, Shaanxi, China.
[2]Qinghai Building and Materials Research Academy Co., Ltd, the Key Lab of Plateau Building and Eco-Community in Qinghai, Xining 810000, Qinghai, China.

*Correspondence to: Prof. Sining Yun, Functional Materials Laboratory (FML), School of Materials Science and Engineering, Xi'an University of Architecture and Technology, No. 13 Yanta Road, Xi'an 710055, Shaanxi, China. E-mail: alexsyun1974@aliyun.com/yunsining@xauat.edu.cn

How to cite this article: Ke T, Yun S, Wang K, Xing T, Dang J, Zhang Y, Sun M, An J, Liu L, Liu J. Constructing bimetal, alloy, and compound-modified nitrogen-doped biomass-derived carbon from coconut shell as accelerants for boosting methane production in bioenergy system. *Energy Mater* 2024;4:400011. https://dx.doi.org/10.20517/energymater.2023.62

Abstract

Accelerants can enhance methane production in biomass energy systems. Single-component accelerants cannot satisfy the demands of anaerobic co-digestion (AcoD) to maximize overall performance. In this work, nitrogen-doped bio-based carbon derived from coconut shells, containing bimetallic Ni/Fe nanoparticles, $FeNi_3$ alloys, and compounds (Fe_2O_3, FeN, and Fe_3O_4), was constructed as hybrid accelerants (Ni-N-C, Fe-N-C, and Fe/Ni-N-C) to boost CH_4 production and CO_2 reduction. The cumulative biogas yield (553.65, 509.65, and 587.76 mL/g volatile solids), methane content (63.58%, 57.90%, and 67.39%), and total chemical oxygen demand degradation rate (60.15%, 54.92%, and 65.38%) of AcoD with Ni-N-C (2.625 g/L), Fe-N-C (3.500 g/L), and Fe/Ni-N-C (2.625 g/L) were higher than control (346.32 mL/g volatile solids, 40.13%, and 32.03%), respectively. These digestates with Ni-N-C, Fe-N-C, and Fe/Ni-N-C showed excellent stability (mass loss: 22.97%-32.75%) and total nutrient content (4.43%-4.61%). Based on the synergistic effects of the different components of the hybrid accelerant, an understanding of the enhanced methanogenesis of AcoD was illustrated.

Keywords: Bio-based carbon, metal-N-C, hybrid accelerant, electron exchange capacity, direct interspecies electron transfer, anaerobic co-digestion, bioenergy

INTRODUCTION

With the rapid growth of cattle farming, cow dung (CD) pollution has become a significant problem. Accumulation of CD leads to the proliferation of a variety of bacteria and pathogens that can seriously affect animal husbandry and human health[1,2]. Therefore, the development of a safe and pollution-free method for handling CD is crucial for environmental protection. Anaerobic digestion (AD) technology is the process of forming combustible mixed biogas and digestate from diverse organic wastes under anaerobic conditions through the decomposition of various microorganisms. However, CD is not suitable as a digestive substrate alone because of its high nitrogen content[3], and the co-digestion of different natural plant wastes and cattle manure has been explored. Aloe is rich in carbon and, as a substrate, can balance C/N of the digestion system[2,4,5]. However, anaerobic co-digestion (AcoD) has drawbacks, including low biogas yield, poor stability, weak growth ability of microorganisms, difficult degradation of stubborn organic matter, and long process cycles[1,6,7]. These problems can be alleviated by applying magnetic fields[3,6], electric fields[8,9], and accelerants[10,11]. Among these methods, adding exogenous accelerants is a practical way to enhance AD performance.

The introduction of metals in AD facilitated the growth of methane-producing bacteria, enhanced degradation of stubborn substrates, and increased biogas yield and yield potential. Córdova-Lizama *et al.* found that Co nanoparticles and zero-valent iron stimulated enzyme activity, promoted the degradation of stubborn substrates, and maintained sufficient stability[12]. Abdelsalam *et al.* reported that zero-valent iron increased biogas and methane production, shortened the lag stage, and stimulated microbial growth[13]. Ke *et al.* reported that Ti spheres promoted the direct interspecies electron transfer (DIET) by accelerating electron transfer between acetogens and methanogens[3]. Zhang *et al.* indicated metals (Fe, Co, Mo, and Ni) improved bioavailability and enhanced stimulative effects of metals on AD[14]. However, excessive addition of Fe and Ni significantly increases virulence to methanogens and decreases their reactivity[15,16]. Therefore, an appropriate amount of metal optimally improves the performance of AcoD.

The biochar has been widely applied in AD owing to its simple processing, low cost, and excellent physical and chemical properties[4,9,17]. Chen *et al.* found that biochar could boost the conversion of ethanol to methane, possibly due to the stimulation of DIET in co-cultures of *Geobacter metallireducens* with *Geobacter sulfurreducens* or *Methanosarcina barkeri*[18]. Wang *et al.* indicated biochar extracted from sawdust can promote methane production and volatile fatty acid (VFA) degradation, confirming that biochar can assist the DIET process[19]. They explored that the biochar prepared from corn straw enhanced the AD performance of kitchen waste, which contributed to enhanced DIET using biochar as an electronic mediator or shuttle[20]. These works proved that biochar can stimulate DIET and promote digestion performance. However, the pristine biochar had a limited effect on CH_4 production and CO_2 reduction.

Because the size of the N atom is equivalent to that of the C atom, N is typically introduced into the carbon matrix to alter its electron distribution[21-26]. Among them, the source of bio-based carbon or biomass-derived carbon included coconut shells, aloe peel, acorn shell, corn cob, sawdust, and walnut shell, and these biomass-derived carbon promoted AD performance[2-6,8,27-30]. Coconut shells, as a widely distributed biomass waste with high carbon content and low ash content, contain high lignin content (30-49 wt.%) and carbon content (53-64 wt.%) and low H/C ratio and O/C ratio, which is very suitable as a carbon source to synthesize the biomass-derived carbon. However, the low stability of N-doped biochar hinders its practical application in real life. Coupling N-doped biochar with metals possesses the potential to enhance its performance. Therefore, many researchers have prepared metal- and N-co-doped biochar; however, most

studies have applied these materials in the field of batteries. Little research has been conducted on degradation of organic contaminants. Xu *et al.* produced Fe/N co-doped biochar extracted from sawdust, which showed excellent oxidative reducibility and high stability owing to its high specific surface area and abundant defects and the synergistic effect between Fe and N doping while achieving efficient degradation of organic pollutants[31]. Li *et al.* studied high stability, reusability, and adaptability of Fe/N co-doped biochar for degradation of various pollutants, thereby increasing its potential for practical applications[32]. Owing to their excellent oxidative reducibility, stability, and degradation properties, metal- and N-co-doped biochar is expected to be used as accelerants in AcoD systems.

Aside from metals and biochar, transition metal compounds promote microbial growth and accelerate electron transfer[33-36]. Li *et al.* found that transition metal carbides increased biogas yield, total chemical oxygen demand (TCOD) degradation rate, and total Kjeldahl nitrogen (TKN) concentration[10]. Jia *et al.* reported that titanium nitride and titanium oxide as electron carriers accelerated electron transfer[6]. Li *et al.* investigated that zero-valent iron nanoparticles stimulated the secretion of proteins and humus in extracellular polymers and promoted the DIET process in AD systems[34]. Wang *et al.* researched W_2N and $W_{18}O_{49}$ as mediators of electron transfer and established an efficient interspecific electrical connection, thus alleviating acidification and enhancing the fermentation performance[37]. However, the reaction conditions of transition-metal compounds are difficult to control, and the reaction sites are limited; the product structure is complex, and the compounds easily aggregate[38]. This suggests that transition metal compounds play a crucial role in promoting digestion performance.

In summary, metal particles, N-doped biochar, and transition metal compounds can boost AD performance by facilitating electron transfer and microbial metabolism in the AD process, whereas an individual accelerant cannot maximize its potential to improve AD performance owing to intrinsic physicochemical shortcomings, including the biotoxicity of excess metal particles and the ready agglomeration of transition metal compounds. Therefore, the objective of this work was to exploit a hybrid accelerant containing metals, carbon, and compounds to explore its synergistic effect on AcoD performance. The effects of the hybrid accelerant on the AcoD were evaluated from biogas production, CH_4 yield, CO_2 reduction, TCOD degradation rate, total solids (TS), volatile solids (VS), thermal stability, and the fertility of the digestate. In addition, mediated electrochemistry was employed to analyze the reduction and oxidation capacity of accelerants. Based on synergistic effects of different components of hybrid accelerants, an understanding of boosted methanogenesis for AcoD systems is illustrated.

EXPERIMENTAL SECTION

Substrate and inoculum

Anaerobic sludge from a wastewater treatment plant in Xi'an was used as the inoculum. The CD was gathered from a breeding farm in Lantian, China, and aloe peel waste was from a beverage processing plant in Yangling, China. The wet weight ratio of 1:3 is based on fresh CD and aloe peel waste as a substrate[2]. Before digestion, fresh CD was domesticated for a week at room temperature. Aloe peel waste was disposed of in water to remove surface dirt, sliced into 1 cm × 1 cm pieces, soaked in 2 M NaOH solution to degrade lignocellulose[4], and then rinsed with water until pH = 7. The detailed characteristics of CD, aloe peel waste, and anaerobic sludge are listed in Table 1.

Preparation of the hybrid accelerant

A N-doped biomass-derived carbon hybrid accelerant was prepared by a simple pyrolysis process, as shown in Figure 1. First, the coconut shell is crushed into a powder of nearly 2 mm in an electric mixer. Then, in a Fe/Ni-N-C synthesis process (red line), 11.16 g $Fe(NO_3)_3 \cdot 9H_2O$ (2.0 mmol, Aladdin, 99.99%), 11.74 g

Table 1. Characteristics of cow dung, aloe peel waste, and anaerobic sludge

Parameters	Cow dung	Aloe peel waste	Anaerobic sludge
Total solids (TS, % Fresh matter)	15.74 ± 0.62	12.23 ± 0.64	4.37 ± 0.10
Volatile solids (VS, % Fresh matter)	12.65 ± 0.42	8.01 ± 0.14	3.70 ± 0.12
VS/TS (%)	80.30 ± 0.49	65.49 ± 0.46	84.67 ± 1.21
Total chemical oxygen demand (TCOD, mg/g Fresh matter)	91.17 ± 0.06	38.20 ± 0.24	43.00 ± 0.62
pH	7.17 ± 0.03	5.79 ± 0.33	7.34 ± 0.41
C (% TS)	52.74 ± 0.39	60.21 ± 0.11	17.43 ± 0.16
H (% TS)	5.46 ± 0.09	11.05 ± 0.36	3.44 ± 0.47
N (% TS)	4.64 ± 0.04	1.77 ± 0.45	2.03 ± 0.07
C/N	11.36 ± 0.37	34.02 ± 0.94	8.59 ± 0.20
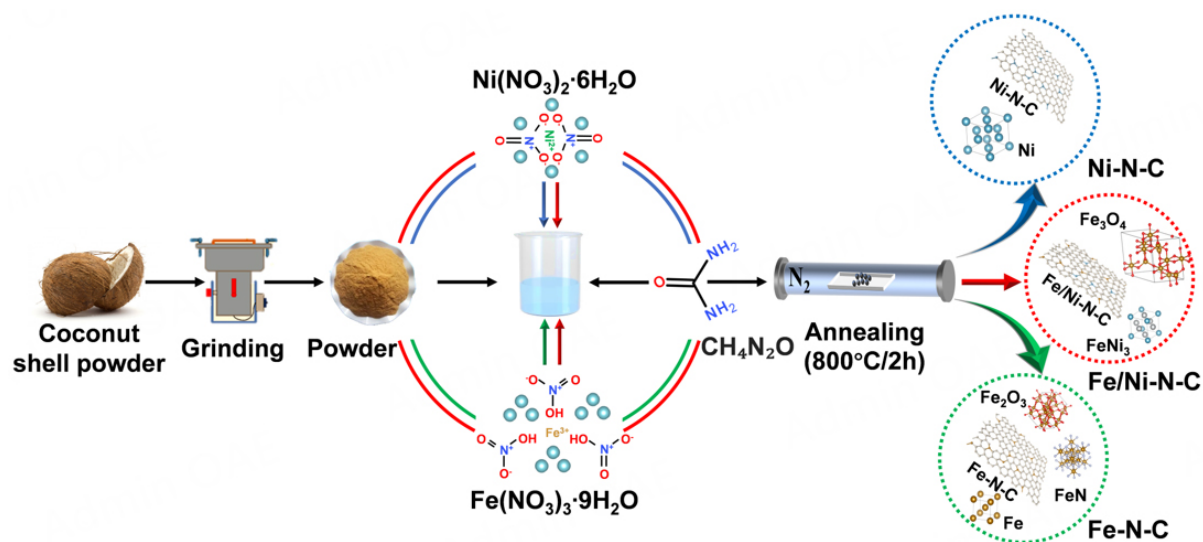
Figure 1. Illustration for the preparation process of Ni-N-C, Fe-N-C, and Fe/Ni-N-C (Blue line: synthesis path of Ni-N-C; Green line: synthesis path of Fe-N-C; Red line: synthesis path of Fe/Ni-N-C).

$Ni(NO_3)_2 \cdot 6H_2O$ (2.0 mmol, Aladdin, 98%), urea (6 g, 16 mmol, Aladdin, 99%), and coconut shell powder (CSP, 6 g) were weighed and completely dispersed in deionized water (50 mL). The solution was stirred in continuous motion for 4 h to mix well. The dried sample at 80 °C was placed at 800 °C for 2 h. Finally, black powder was obtained and named Fe/Ni-N-C. Following the established process, 11.74 g $Ni(NO_3)_2 \cdot 6H_2O$ and 11.16 g $Fe(NO_3)_3 \cdot 9H_2O$ as metal precursors were added in the synthesis process of Ni-N-C (blue line) and Fe-N-C (green line), respectively, and kept other steps and processes same. Detailed sample characterization means can be found in the Supplementary Material.

Experimental set-up

Batch experiments were tested in glass bottles with an effective volume of 400 mL in a constant temperature water bath at 37 °C for 35 days. Previous work has reported an optimal substrate-to-inoculum ratio of 3:7[2,39]. Ni-N-C, Fe-N-C, and Fe/Ni-N-C as accelerants were added in digesters, where the dosage of each accelerant in the reactors was 0.875, 1.750, 2.625, and 3.500 g/L, respectively. No accelerants were added to the control group. To ensure the veracity of the experiment, all batches were repeated twice. Kinetic analysis of biogas production can be found in the Supplementary Material.

Statistical analysis

SPSS software was used to perform statistical analysis. The differences in experimental data are evaluated by using one-way analysis of variance (ANOVA), and a *P* value lower than 0.05 ($P < 0.05$) was considered as a significant difference.

RESULTS AND DISCUSSION

Characteristics of materials

The X-ray powder diffractometer (XRD) results are shown in Figure 2A-C. Ni-N-C, Fe-N-C, and Fe/Ni-N-C exhibit a peak at 26°, representing the (002) plane of graphitic carbon. The diffraction of carbon support in the accelerant does not show clearly in the XRD data, which may be due to the strong peaks of Ni, Fe, $FeNi_3$, and other metal compounds covering the diffraction of carbon. Similar situations have been reported in the previous literature[25,31]. Ni-N-C has three peaks (JCPDS: 70-1849) at 45°, 52°, and 76°, responding to the (111), (200) and (220) lattice planes of Ni, respectively. The two distinct characteristic peaks occurring at 45° and 65° of Fe-N-C are attributed to (110) and (200) lattice planes of Fe (JCPDS: 87-0722), respectively. The characteristic peaks appear at 44°, 51° and 76° in Fe/Ni-N-C, matching with the (111), (200), and (220) lattice surfaces of the $FeNi_3$ alloy (JCPDS: 88-1715), respectively. Due to the different diameters of Fe and Ni atoms, the strain in the crystal lattice increased the surface energy and, thus, enhanced redox properties and electron mobility of the $FeNi_3$ alloy[25,40]. The remaining impurity characteristic peaks pattern of Fe-N-C originate from Fe_2O_3 (JCPDS: 73-0603) and FeN (JCPDS: 75-2127). In addition, Fe_3O_4 (JCPDS: 75-1609) of Fe/Ni-N-C accelerants may be due to the redox reaction between the pyrolysis and biological carbon[31,41,42]. As expected, bimetal, alloy, and compound-modified nitrogen-doped biomass-derived carbon was successfully constructed.

The Raman spectra of three accelerants exhibit the D-band at 1,340-1,360 cm^{-1} and the G-band at 1,580-1,610 cm^{-1}, respectively, as shown in Figure 2D. The D band is for defective sites or disordered sp^3 hybridized carbon, and the G band is for ideal sp^2 hybridization of C-C bonds in the graphite phase[43-45]. In order to clearly understand the property of the as-prepared bio-carbon, the curve fitting method of Gauss-Lorentz numerical simulation was used to deconvolve[46,47]. The I_{D_1}/I_G ratio of Ni-N-C, Fe-N-C, and Fe/Ni-N-C decreased from 1.54 to 1.17 to 0.95 [Figure 2E-G], indicating that Fe/Ni-N-C has a high degree of the graphitization [Figure 2H], which can lead to fast electron transfer between microorganisms[48-50].

The microstructure of hybrid accelerants was determined by field emission scanning electron microscope (FESEM), which has an obvious stacking layer and wrinkle morphology, as depicted in Figure 3A-C. The transmission electron microscope (TEM) and high resolution TEM (HRTEM) of Ni-N-C, Fe-N-C, and Fe/Ni-N-C are displayed in Figure 3D and E, Figure 3F and G, and Figure 3H and I, respectively. The inverse Fast Fourier Transform (IFFT) image of the (111) facet of Ni of Ni-N-C is given in Supplementary Figure 1A, where the lattice distance of 0.2050 nm relates to the (111) face of Ni [Figure 3J]. The Fast Fourier Transform (FFT) and IFFT images with corresponding red boxes in Figure 3F and G are indicated in Supplementary Figure 1B-D, respectively. The lattice spacing is 0.2466, 0.2019, and 0.2047 nm on the (110), (111), and (110) faces of Fe, FeN, and Fe_2O_3 [Figure 3J], respectively. The lattice distances of 0.2486 and 0.2089 nm coincide with (111) and (103) planes of $FeNi_3$ and Fe_3O_4 of Fe/Ni-N-C [Figure 3J], respectively, as depicted in the IFFT images in Supplementary Figure 1E and F. Figure 3K shows the attached energy dispersion spectrometer (EDS) mapping images of Fe/Ni-N-C. The elements C, N, O, Fe, and Ni are evenly spaced in Fe/Ni-N-C.

Furthermore, the relevant components of hybrid accelerants are further verified through X-ray photoelectron spectroscope (XPS) measurement. Ni, Fe, C, N, and O can be identified from the full
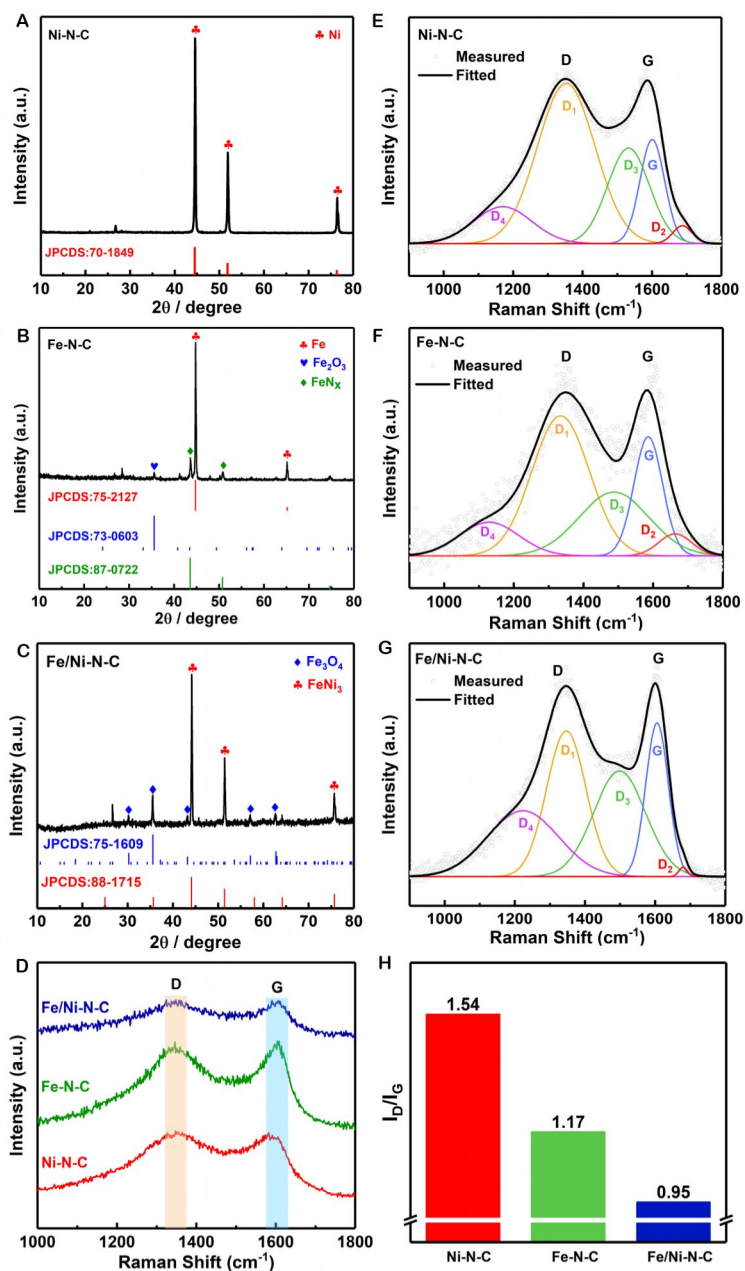
Figure 2. (A-C) XRD patterns of Ni-N-C, Fe-N-C, and Fe/Ni-N-C, (D) Raman spectra, (E-G) fitted curves of Raman spectra, and (H) the ratio of I_D/I_G of Ni-N-C, Fe-N-C, and Fe/Ni-N-C.

spectrum of XPS [Figure 4A]. The Fe 2p spectrum of Fe-N-C and Fe/Ni-N-C shows two obvious asymmetric bands, namely the low energy (Fe $2p_{1/2}$) band and high energy (Fe $2p_{3/2}$) band in Figure 4B and C. Fe 2p is classified as metallic iron (Fe^0, 708.9 and 709.4 eV), Fe^{2+} $2p_{3/2}$ (710.4 and 711.2 eV), Fe^{3+} $2p_{3/2}$ (712.4 and 714.7 eV), metallic iron (Fe^0, 718.0 and 719.0 eV), Fe^{2+} $2p_{1/2}$ (723.8 and 723.7 eV), and Fe^{3+} $2p_{1/2}$ (726.2 and 726.2 eV). The XPS spectrum of Ni-N-C and Fe/Ni-N-C Ni 2p [Figure 4D and E] has six forms of Ni: Ni^0 $2p_{3/2}$ (852.6 and 852.4 eV), Ni^0 $2p_{1/2}$ (869.2 and 869.5 eV), Ni^{2+} $2p_{3/2}$ (855.4 and 855.6 eV), Ni^{2+} $2p_{1/2}$ (872.9 and 873.3 eV), and two satellite peaks (861.0 and 861.2 eV, 879.4 and 879.2 eV). This proved that the accelerants consist of a carbon skeleton anchored by Ni-N$_X$ or Fe-N$_X$ groups with Ni or Fe embedded in them. Results are familiar to the previous work[25,51].
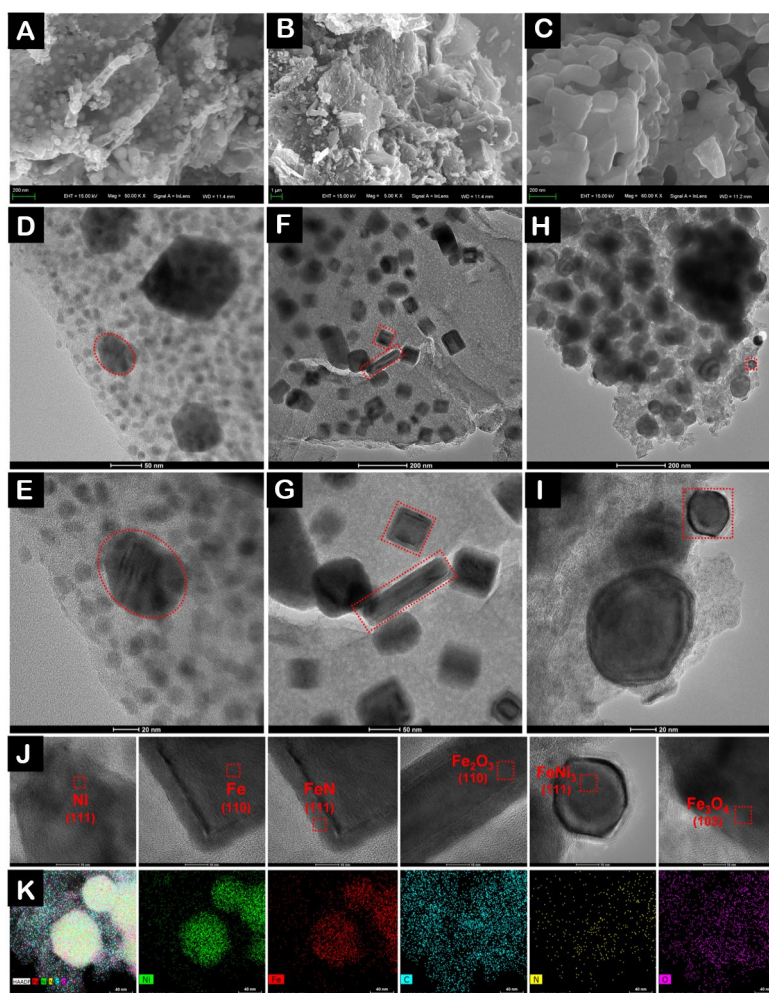
Figure 3. (A-C) SEM images. (D and E) TEM and HRTEM images of Ni-N-C. (F and G) TEM and HRTEM images of Fe-N-C. (H and I) TEM and HRTEM images of Fe/Ni-N-C. (J) HRTEM images for the (111) planes of Ni of Ni-N-C, HRTEM images for (110), (111), and (110) planes of Fe, FeN, and Fe_2O_3 of Fe-N-C, HRTEM images for (111) and (103) planes of $FeNi_3$ and Fe_3O_4 of Fe/Ni-N-C. (K) EDS mapping images of Fe/Ni-N-C.

The N 1s spectrum of Ni-N-C, Fe-N-C, and Fe/Ni-N-C in Figure 4F-H was fitted to five sub-peaks, namely pyridinic-N (~398.5 eV), pyrrolic-N (~400.9 eV), graphitic-N (~401.8 eV), oxidized-N (~403.2 eV), and Ni/Fe-N (~399.2 eV)[24,52]. The presence form and atomic percentage of N are shown and listed in Figure 4I and Supplementary Table 1 to reveal the differences of N types. The increase in pyridinic-N and pyrrolic-N could improve Fe/Ni-N-C accelerants activity[43,44,53-56]. The findings can be confirmed in the electron exchange capacity (EEC). C 1s spectra [Supplementary Figure 2] were fitted as C=O (~288.8 eV), C-N (~285.5 eV), and C-C (~284.8 eV)[41,57]. The presence of C-N reveals successful N doping. C=O will accelerate the electron transfer rate and promote direct interspecific electron transfer[58,59].

AcoD performance

Biogas production, CH_4 and CO_2 content

The daily biogas yield obtained by adding different concentrations of accelerants in AcoD systems is shown in Figure 5A-C. Throughout the digestion process, there are two representative peaks; the first peak represents the decomposition of hydrocarbons, and the second peak represents the consuming decomposition of complex crude proteins, as proved in the previous works[5,29,37]. The first peak occurred on
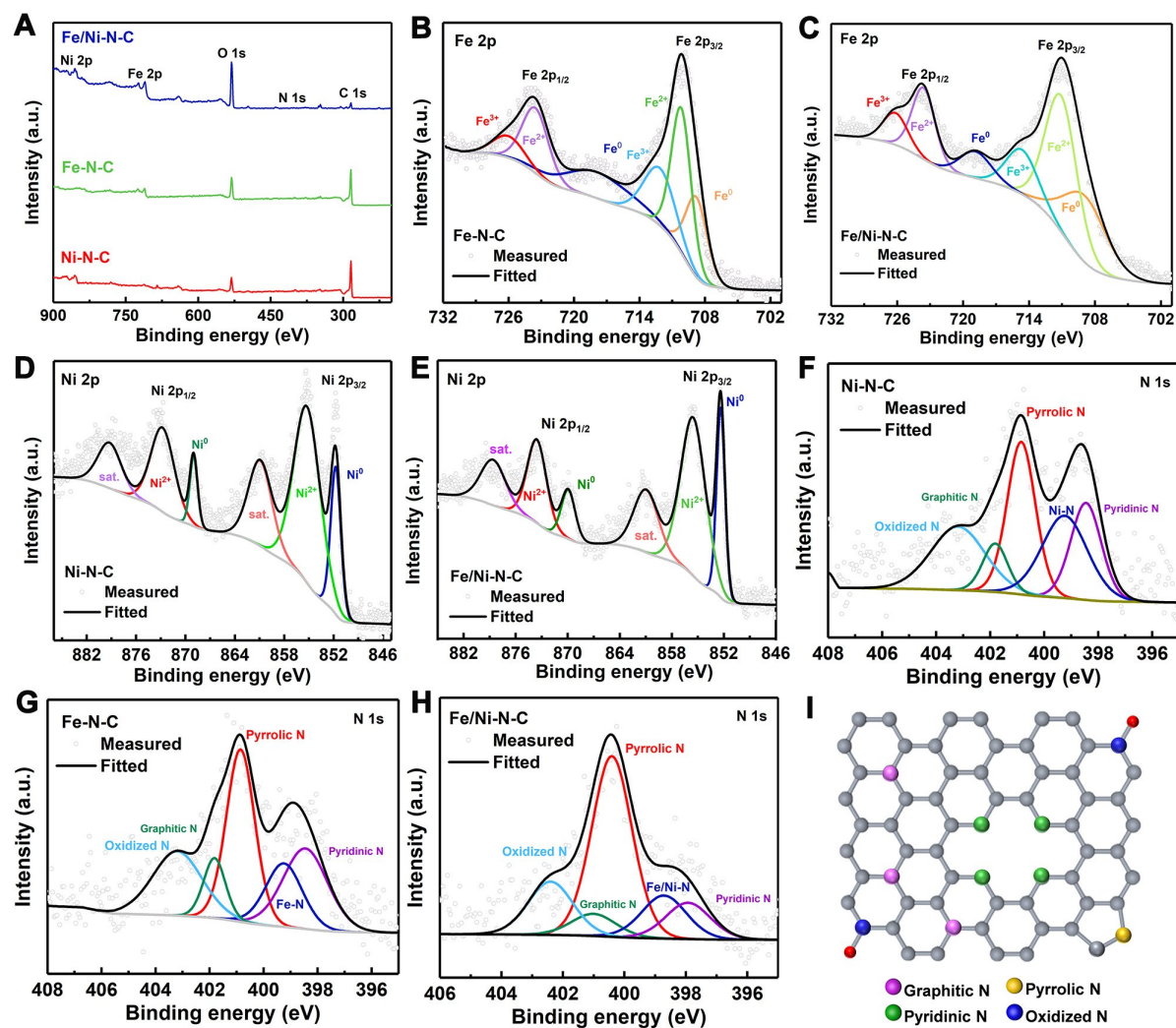
Figure 4. (A) XPS measurement spectra, (B and C) Fe 2p XPS spectra of Fe-N-C and Fe/Ni-N-C, (D and E) Ni 2p XPS spectra of Ni-N-C and Fe/Ni-N-C, (F-H) N 1s XPS spectra of Ni-N-C, Fe-N-C, and Fe/Ni-N-C, and (I) schematic diagram of different N types.

days 9-12, days 7-12, and days 10-14, and the second peak occurred on days 21-22, days 14-19, and days 17-25 with the different concentrations of Ni-N-C, Fe-N-C, and Fe/Ni-N-C, respectively. The first and second daily biogas production peaks [Figure 5A-C] of Ni-N-C (28.76-36.73 and 27.43-28.98 mL/g VS), Fe-N-C (28.76-32.82 and 25.19-33.00 mL/g VS), and Fe/Ni-N-C (31.34-39.09 and 28.24-34.29 mL/g VS) were clearly higher than control (22.95 and 19.43 mL/g VS). These results suggested hybrid accelerants may facilitate degradation of stubborn matter, accelerate the co-digestion process, and increase biogas production.

The results of the cumulative biogas yield experiments were fitted using modified Gompertz models [Figure 5D-F], with kinetic parameters shown in Supplementary Table 2. The predicted biogas yield values (415.11-522.19 mL/g VS with Ni-N-C, 427.54-545.58 mL/g VS with Fe-N-C, and 520.70-612.34 with Fe/Ni-N-C) closely approached the measured cumulative biogas yield (402.95-509.92 mL/g VS with Ni-N-C, 409.22-553.65 mL/g VS with Fe-N-C, and 494.69-587.76 mL/g VS with Fe/Ni-N-C, in Figure 5G). R^2 ranged from 0.9983-0.9999, indicating that the experimental data are within a reasonable range. Obviously, all the groups of Ni-N-C, Fe-N-C, and Fe/Ni-N-C can improve biogas production as compared to the control.
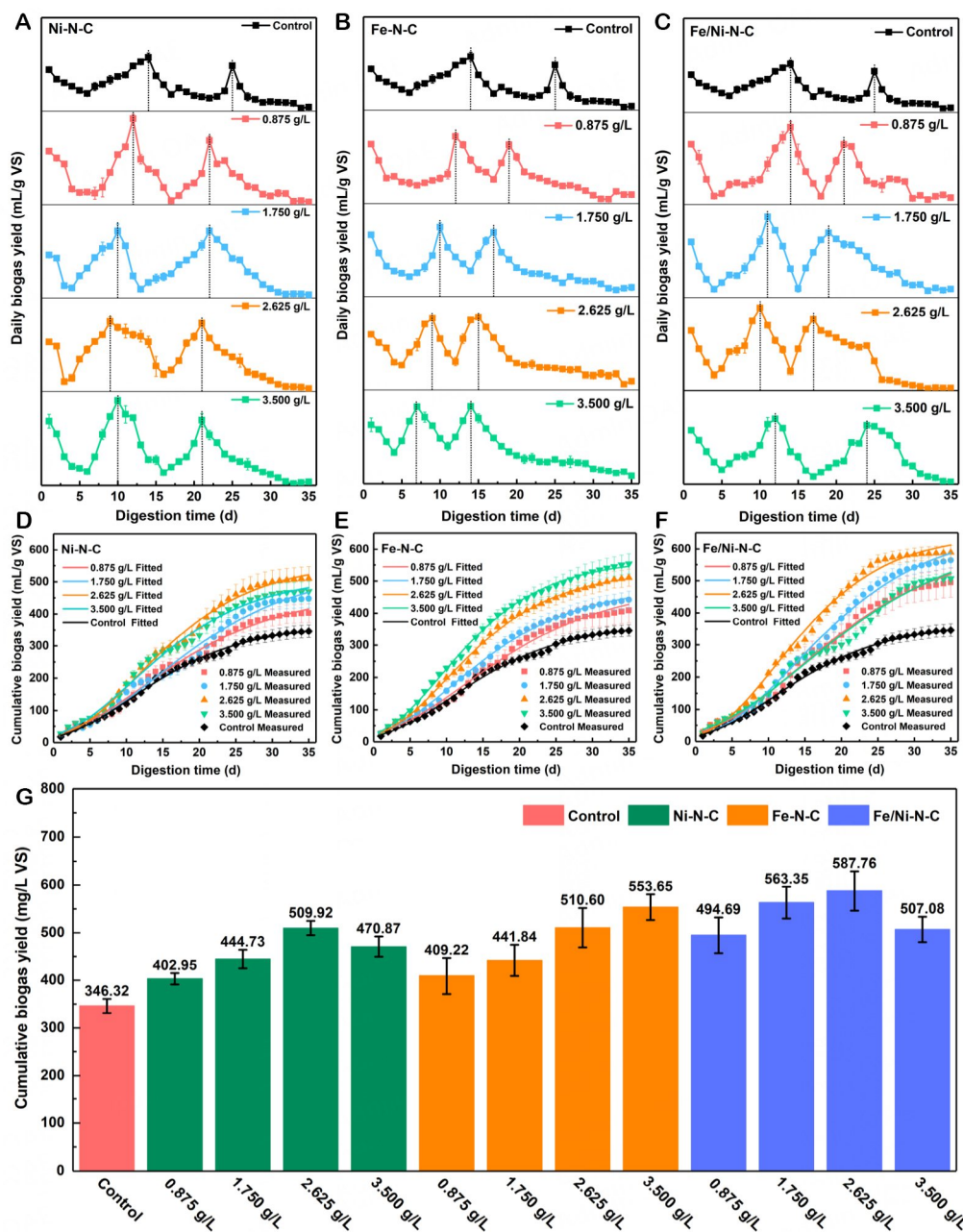
Figure 5. (A-C) Daily biogas yield, (D-F) measured and fitted cumulative biogas production, and (G) cumulative biogas yield of AcoD systems with Ni-N-C, Fe-N-C, and Fe/Ni-N-C.

Furthermore, CH_4 and CO_2 contents were measured for the experimental group supplemented with 2.625 g/L Ni-N-C (57.90% and 27.85%), 3.500 g/L Fe-N-C (63.58% and 25.62%), 2.625 g/L Fe/Ni-N-C (67.39% and 16.97%), and the control (40.13% and 34.96%), as shown in Figure 6. The contents of CH_4 and CO_2 measured were within the normal range of 35%-70% and 15%-50%, respectively, as recorded in the previous reports[60], which implies that introducing hybrid accelerants in the AcoD systems promotes conversion of CO_2 to CH_4. These results indicated that hybrid accelerants can indeed improve AcoD
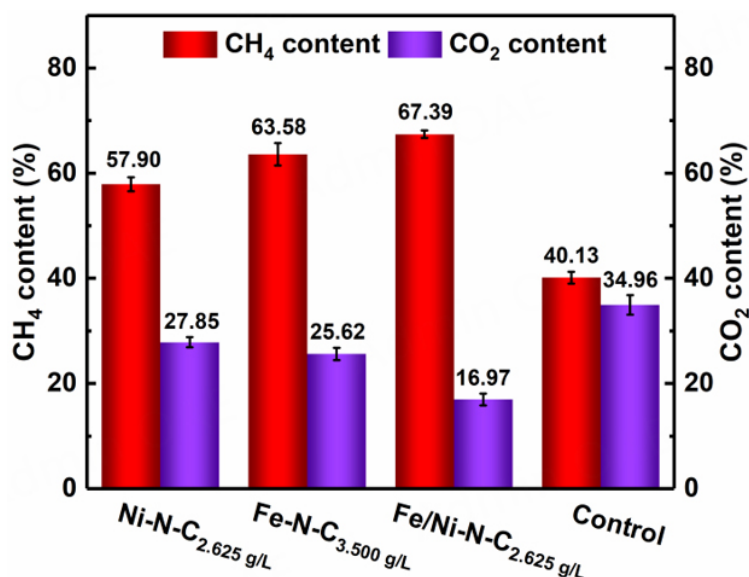
Figure 6. Average CH_4 and CO_2 contents of the AcoD systems with Ni-N-C, Fe-N-C, and Fe/Ni-N-C accelerants.

performance. The boosted methanogenesis of hybrid accelerants in AcoD is discussed in Section "Understanding of enhanced methanogenesis pathway in AcoD systems".

pH values, TCOD degradation rate, TS, and VS reduction

The change in pH value is presented in Figure 7A-C. All digestion systems showed similar trends. The initial pH values of different experimental groups varied between 7.12 and 7.34. In the first five days of digestion, pH is reduced, which may be caused by the decomposition and acidification of readily degradable organic matter[10,11,61]. Subsequently, pH began to rise in all the digesters. During the whole co-digestion process, all pH values varied between 6.27-7.59, which was within the appropriate range of 5.5-8.2 for the acetogenesis and methanogenesis[39,62,63]. However, the pH of digesters with accelerants was higher than the control on days 5-10, possibly because the buffer capacity of the non-accelerant system is weak. TCOD degradation rates (41.19%-54.92% for Ni-N-C, 36.39%-60.15% for Fe-N-C, and 49.69%-65.38% for Fe/Ni-N-C) of the accelerant-added digesters were higher than that of the control (32.03%), as presented in Figure 7D-F and Supplementary Table 3. In addition, 2.625 g/L Fe/Ni-N-C obtained the highest TCOD degradation rate (65.38%). In this work, the initial chemical oxygen demand (COD) was 59,740.86 mg/L, and the final COD ranged from 20,683.86 to 40,602.93 mg/L, which resulted in the COD reduction of 19,137.93-39,057.00 mg/L. According to the theoretical methane yield (0.35 L/g COD) in the previous literature[1,9], the required COD corresponding to cumulative biogas yields ranged from 13,417.43 to 22,771.50 mg/L [Supplementary Table 4]. The loss of TCOD in each reactor can be attributed to the production of carbon dioxide and other organic matter[64]. This result was consistent with that of biogas production and methane content, demonstrating that adding hybrid accelerants can facilitate the degradation of organic compounds. The biogas yield and TCOD degradation rate with Ni-N-C, Fe-N-C, and Fe/Ni-N-C are also comparable to those reported in the previously published work [Supplementary Table 5].

As shown in Figure 8, the initial TS and VS of digestate before digestion were 73.60 and 39.01 g/kg, respectively. TS and VS contents decreased as organic matter began to degrade. At the end of digestion, TS and VS contents remained stable. Then, TS and VS contents were monitored to calculate their reduction. TS
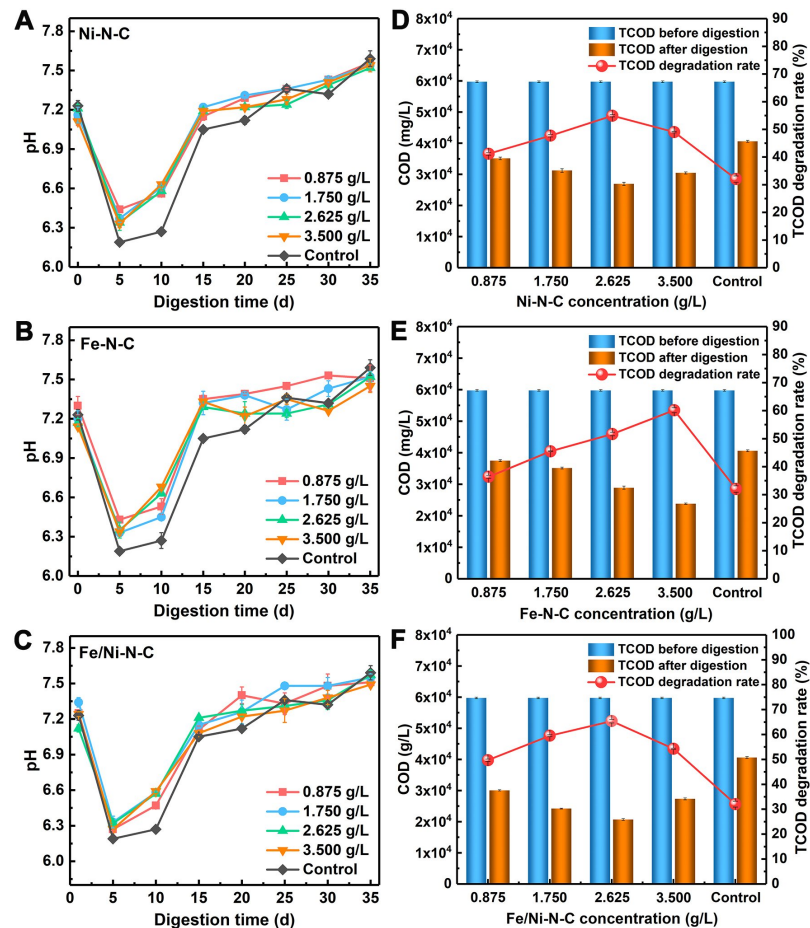
Figure 7. (A-C) pH values variation and (D-F) TCOD degradation rate of AcoD systems after adding Ni-N-C, Fe-N-C, and Fe/Ni-N-C.

and VS reductions were 34.64%-38.48% and 42.51%-51.59% for Ni-N-C, 38.06%-45.60% and 49.19%-55.39% for Fe-N-C, and 42.59%-62.92% and 51.78%-64.47% for Fe/Ni-N-C, 29.64 and 44.85% for the control group in AcoD systems, respectively, as shown in Supplementary Table 3. These results indicated that hybrid accelerants can promote the organic matter degradation of co-substrate, and the bimetallic accelerant showed a better promotion effect on substrate degradation ($P < 0.01$, in Supplementary Table 6).

According to the economic analysis in the previous literature[1,64], by comparing the cost of these accelerants to the income generated from the increased biogas production, these accelerants are not cost-effective. However, this analysis did not take into account the overall benefits as a whole system. For example, these accelerants can reduce COD and solids content, resulting in lower costs for storage and transport of digestate in the industrial-scale biogas plant. The digestate can act as one component of a compound fertilizer, offering an option to reduce the cost of accelerants. In large-scale biogas plants, utilizing the biogas generated for cogeneration can result in additional economic and environmental benefits. Furthermore, to develop renewable energy and combat environmental pollution, the government is introducing policies to reduce the cost and tax burden of large biogas plants.

Digestate performance
Digestate stability
After the digestion, based on excellent biogas production and co-substrate degradation, the digestates with
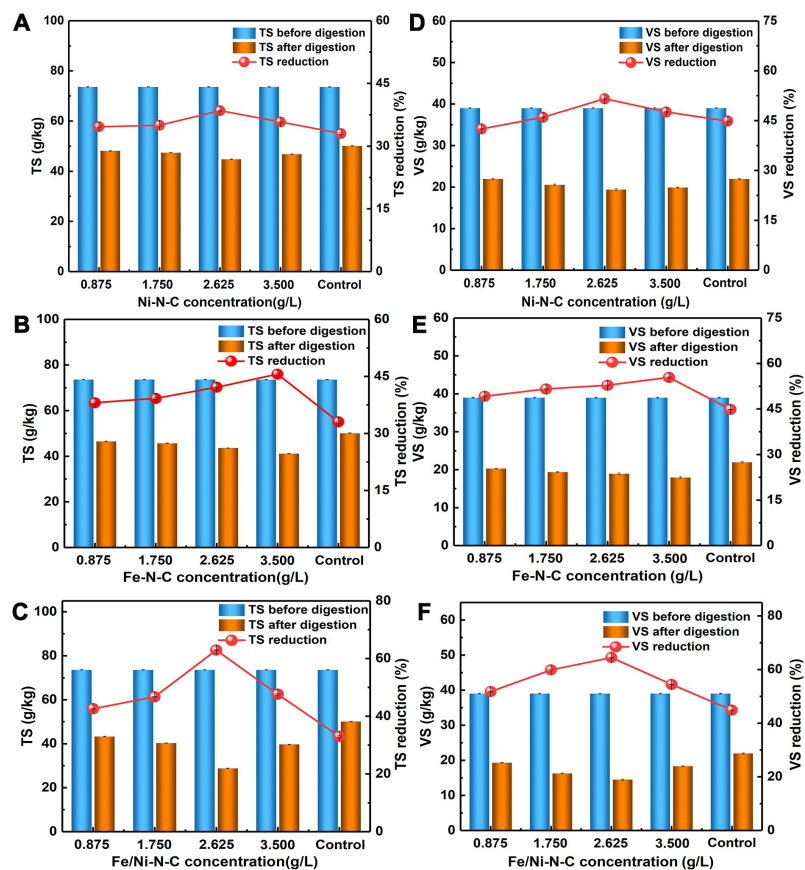
Figure 8. (A-C) TS reduction and (D-F) VS reduction of AcoD systems after adding Ni-N-C, Fe-N-C, and Fe/Ni-N-C.

hybrid accelerants of the optimal concentration (2.625 g/L Ni-N-C, 3.500 g/L Fe-N-C, and 2.625 g/L Fe/Ni-N-C) were tested for thermogravimetric analyses. Figure 9A-C shows thermogravimetry (TG), mass loss, and differential thermogravimetry (DTG) for hybrid accelerants and the control group. The TG curve is split into three stages according to the DTG curve and increases gradually with temperature. The first stage (below 100 °C) of mass loss corresponded to the first peak of the DTG curve and was mainly due to the release of water[61,63]. The most important stage of the TG curve is the second stage (200-400 °C), corresponding to the second peak (about 270 °C), which is correlated with the degradation of carbohydrates, hemicellulose, and aliphatic groups[28,37]. The digestate of 2.625 g/L Ni-N-C (18.62%), 3.500 g/L Fe-N-C (15.25%), and 2.625 g/L Fe/Ni-N-C (11.53%) showed a lower mass loss in the second stage than the control group (28.54%). The third stage corresponds to the third (about 450 °C) and fourth peaks (about 630 °C), occurring across the range 400-700 °C, which is relevant to the decomposition of lignocellulose[1,61]. The total mass loss was 32.75% for Ni-N-C, 29.36% for Fe-N-C, 22.97% for Fe/Ni-N-C, and 46.74% for the control. Mass loss of the hybrid accelerants was lower than that of the control, which states that the organic matter in digestate added with accelerants degraded more completely. Two obvious exothermic peaks were observed in the differential scanning calorimetry (DSC) curve [Figure 9D]. The first exothermic peak (300-350 °C) was due to decay of simple organic matter, and the second exothermic peak (450-500 °C) was owing to degradation of complex organic matter[10]. According to thermogravimetric analyses, the addition of hybrid accelerants to AcoD systems improved catabolism of recalcitrant matter.
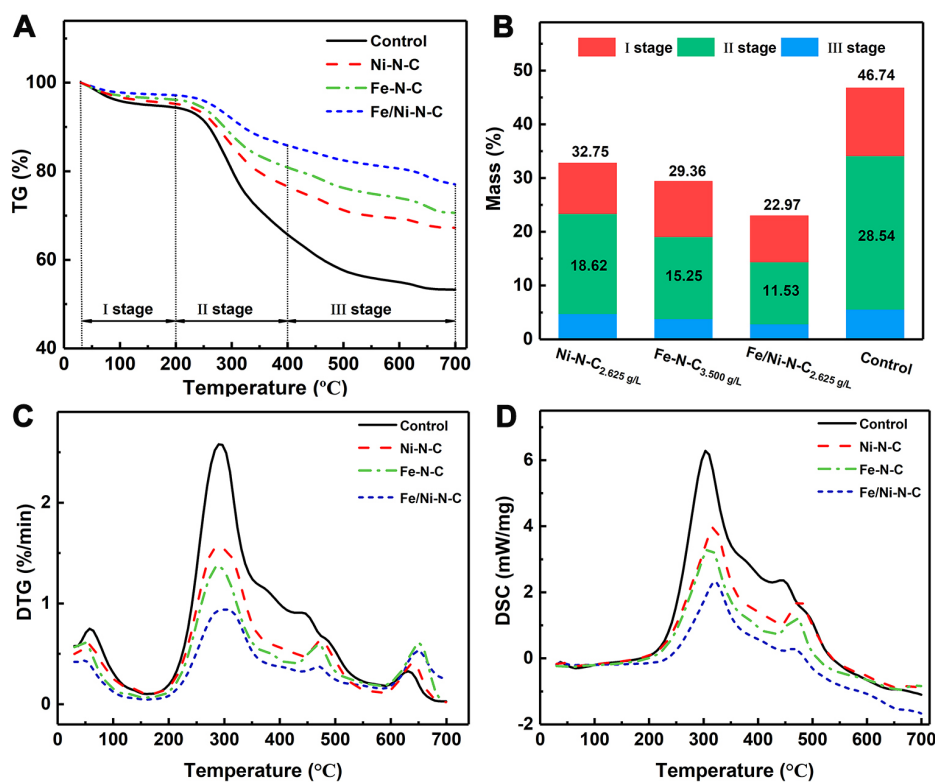
Figure 9. (A) TG, (B) Mass loss, (C) DTG, and (D) DSC profiles for the digestate in AcoD systems with accelerants of Ni-N-C, Fe-N-C, and Fe/Ni-N-C.

Nutrient content of the digestate

Fertility was evaluated by measuring TK, TP, and TN contents in 2.625 g/L Ni-N-C, 3.500 g/L Fe- N-C, and 2.625 g/L Fe/Ni-N-C digestate [Table 2]. The total nutrient contents of Ni-N-C, Fe-N-C, and Fe/Ni-N-C digestate were 4.46%, 4.61%, and 4.43%, respectively, which were higher than that of soil. In addition, according to the NY525-2021 standard of the Ministry of Agriculture of the People's Republic of China, the total nutrient mass fraction (on a dry basis) of organic compound fertilizers must be 4% and above[65,66], which makes the addition of hybridization enhancers as digestate for organic fertilizers promising. In addition, as summarized in Table 2, the total nutrient contents of Ni-N-C, Fe-N-C, and Fe/Ni-N-C digestate were also higher than those (3.54%-3.64%) of the digestate without accelerants[8,9]. The effect of bimetallic accelerants and monometallic accelerants makes no big difference, which may be due to the fact that the substrate in AD systems is the same, and the NPK content in the bimetallic accelerant and monometallic accelerant is not significantly different. In general, digestate can be used as a compound fertilizer to improve soil fertility, improve crop quality, and maintain soil fertility. According to the Chinese risk control standard for soil contamination of agriculture land (GB15618-2018) and the organic fertilizer standard (NY525-2021, China), heavy metal pollutants mainly include Hg, Cr, Pb, Cu, As, and Cd, and most listed heavy metals have the upper limit of higher than 15 mg/kg in soil except for Cd and Hg. Fe and Ni elements are not listed in the risk control standard, and their concentration would also not exceed the risk control standard. Therefore, the digestates with residual nitrogen-doped biomass-derived carbon would not cause environmental risks[3]. Actually, addition of carbon-based byproducts in soil is gaining popularity as a plant growth stimulator, soil quality enhancer, and fostering green land vegetation[67,68]. Therefore, the utilization of digestate as a carbon-based fertilizer can further enhance its added value.

Table 2. The effect of Ni-N-C, Fe-N-C, and Fe/Ni-N-C accelerants on fertility of digestate

Experiments	TN (g/kg)	TK (g/kg)	TP (g/kg)	Total nutrient content (%)	Ref.
Soil	0.15-0.20	0.06-0.10	0.10-0.15	0.31-0.45	[10]
Bioorganic fertilizer	17.10	25.40	18.00	6.05	[39]
NY525-2021	-	-	-	4.00	Chinese agricultural standard
Digestate (CK)	-	-	-	3.64	[8]
Digestate (CK)	17.07 ± 0.12	6.48 ± 0.36	11.80 ± 0.08	3.54 ± 0.21	[9]
Digestate (BC)	15.60 ± 0.15	11.62 ± 0.21	6.45 ± 0.22	3.37 ± 0.58	[4]
Digestate (Ti$_{MF}$)	20.80 ± 0.22	6.51 ± 0.04	14.86 ± 0.21	4.21 ± 0.40	[3]
Digestate (Ni-N-C)	21.31 ± 0.11	13.06 ± 0.18	10.23 ± 0.21	4.46 ± 0.50	This work
Digestate (Fe-N-C)	21.66 ± 1.67	11.57 ± 0.06	12.86 ± 0.21	4.61 ± 0.18	This work
Digestate (Fe/Ni-N-C)	21.22 ± 0.13	12.41 ± 0.19	10.74 ± 0.21	4.43 ± 0.53	This work

Mediated electrochemical analysis

Figure 10A-C showed the reduction and oxidation current peaks of Ni-N-C, Fe-N-C, and Fe/Ni-N-C in mediated electrochemical reduction (MER) and oxidation (MEO), respectively. The number of transferred electrons (Q) and the mass of the accelerants are highly correlated (R^2 > 0.95) [Figure 10D-F]. Fe/Ni-N-C exhibited the highest electronic exchange capacity (EEC = electron accepting capacity (EAC) + electron donating capacity (EDC), 1.09 μmol e$^-$/g), followed by Ni-N-C (1.07 μmol e$^-$/g) and Fe-N-C (1.05 μmol e$^-$/g). The EEC of Ni-N-C (1.07 μmole$^-$/g), Fe-N-C (1.05 μmol e$^-$/g), and Fe/Ni-N-C (1.09 μmole$^-$/g) accelerants surpassed that of previously reported biomass-derived carbon accelerants without metal sites[4,9], especially, 0.62 μmol e$^-$/g for coconut-shell-derived carbon, 0.31 μmol e$^-$/g for aloe peel-derived carbon, 0.66 μmol e$^-$/g for N, S co-doped aloe peel-derived carbon, and 0.65 μmol e$^-$/g for N, P co-doped aloe peel-derived carbon, which could confirm the significant promotion effect of the monometallic and bimetallic accelerant on the electron transport of AD systems with accelerants.

Understanding of enhanced methanogenesis pathway in AcoD systems

This work herein briefly introduced the AcoD process. AcoD is involved in the nutrient metabolism in various bacteria[69]. In the hydrolysis stage, recalcitrant substances are broken down into soluble monomers; in the acidification stage, acetogens metabolize hydrolytic products to acetic acid, hydrogen, and carbohydrates; in the methanogenesis stage, acidification products are converted to CH_4 by methanogens. To understand the role of the hybrid accelerant in AcoD systems, a possible strategy was proposed [Figure 11]. Depending on the metabolism of methanogens, methanogenesis can be divided into acetate-dependent CH_4 production (Route I: $CH_3COO^- + H^+ \rightarrow CH_4 + CO_2$), H_2-dependent CH_4 production (Route II: $4 H_2 + CO_2 \rightarrow CH_4 + 2 H_2O$), and electron-dependent CH_4 production (Route III: $8 H^+ + 8 e^- + CO_2 \rightarrow CH_4 + 2 H_2O$)[37,70]. The relatively slow nutrient metabolism of soluble monomers in Route I limited the digestion efficiency of AcoD systems[71]. Route II uses H_2 as an electron carrier between hydrogen-producing to transfer electrons, known as interspecies hydrogen transfer (IHT). The diffusion of H_2 is slow, and the slight interruption of H_2 disrupts the nutritional metabolic balance, leading to the accumulation of organic acids and inhibiting the formation of CH_4. Route III, also known as DIET, is a process in which digestion bacteria directly transfer electrons to methanogens.

As shown in Figure 11, CH_4 production depends on Route I and Route II in the AD system without accelerants. After adding accelerants, in addition to enhancing Route I and Route II, Route III is proposed. The enhanced methanogenesis was attributed to the enhanced DIET process. Conductive materials can create a bioelectric link between acetogens and methanogens. On the one hand, electron carriers facilitate e$^-$ transfer between acetogen and methanogens (Route II); on the other hand, conductive materials enhance the transfer of H^+ and e$^-$ (Route III), as has been demonstrated previously[3,6,7,72,73].
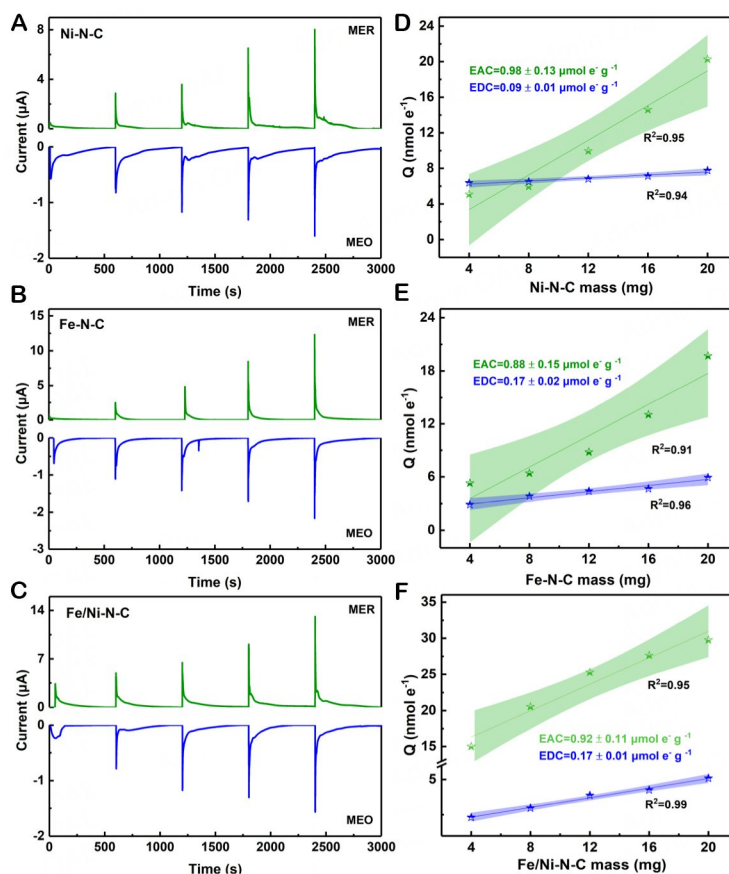
Figure 10. (A-C) Electron exchange capacity and (D-F) transferred electron number of Ni-N-C, Fe-N-C, and Fe/Ni-N-C accelerants.
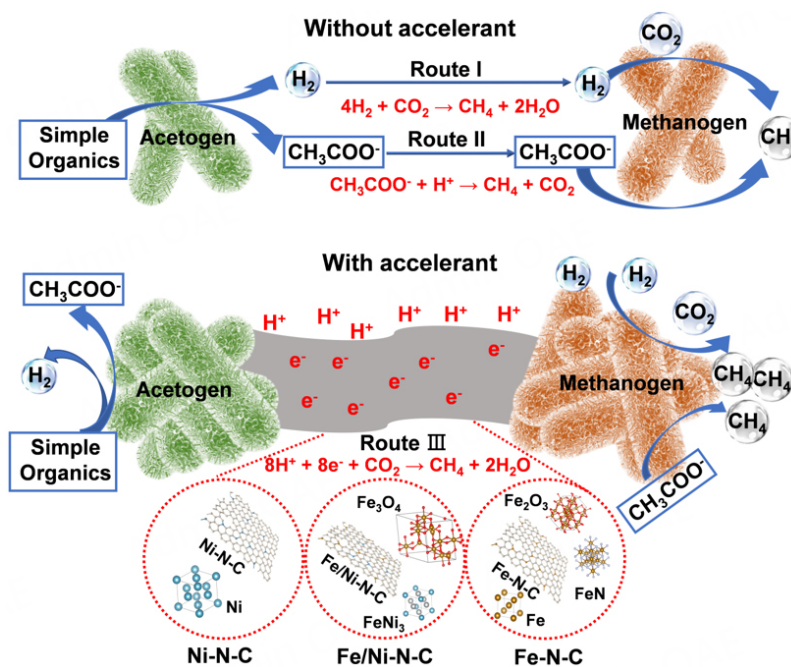

Figure 11. Schematic for understanding enhanced CH_4 production and CO_2 reduction in AcoD systems without and with accelerants.

In this work, N-doped biomass-derived carbon, bimetallic Ni/Fe nanoparticles, and $FeNi_3$ alloys are conductive materials. N-doped biomass-derived carbon containing bimetallic Ni/Fe nanoparticles and $FeNi_3$ alloys as accelerants enhanced methanogenesis. On the other hand, the hybrid accelerant has a high degree of graphitization [Figure 2] and forms many $Fe-N_x$ and $Ni-N_x$ active sites on the surface [Figure 4], which may promote electron transfer between microorganisms. On the other hand, pyridinic-N and pyrrolic-N can promote EDC, and C=O can promote charge transfer between microorganisms and matter in the substrate, enhancing EAC[4,53,56]. Therefore, hybrid accelerants have strong EEC (1.05-1.09 μmol e⁻/g), which can reduce CO_2 to CH_4, which is confirmed by CH_4 content analysis (hybrid accelerants: 57%-68%, control: 40.13%). For the hybrid accelerants constructed, N species (pyridinic-N, pyrrolic-N, and graphitic-N) are the active sites for the adsorption and activation of CO_2[74]. In addition, dual-metal sites could promote CO_2 adsorption[75]; metal species could maximize the use of atoms, and electron-enriched metal sites acted as highly active sites to activate CO_2[76]. Therefore, the synergistic effect of hybrid accelerants improves the adsorption and activation capacity of CO_2. Bimetallic Ni/Fe nanoparticles and $FeNi_3$ alloys of hybrid accelerants can stimulate the DIET process and promote CH_4 production.

In addition, compounds (Fe_2O_3, FeN, and Fe_3O_4) in the hybrid accelerant can release Fe^{2+} and Fe^{3+} to break down the chemical bonds of recalcitrant organic matter into simpler organic molecules, providing more substrates for methanogens; simultaneously, the released metal ions promote metal enzymes activity, providing necessary nutrients for microorganisms to promote their growth and metabolism, further promoting methane production, which has been verified in previous studies[3,4].

Based on the above analysis, the improvement of AcoD performance by biomass-derived carbon hybrid accelerant is due to the synergistic effect of different components of bimetallic Ni/Fe nanoparticles, $FeNi_3$ alloys, and compounds (Fe_2O_3, FeN, and Fe_3O_4). In the future, more experiments will be carried out to study the synergistic effect of accelerants and microorganisms by using sludge + peel waste and also model chemicals such as CH_3COOH, CH_4, and CO_2.

CONCLUSIONS

Nitrogen-doped biomass-derived carbon hybrid accelerants (Ni-N-C, Fe-N-C, and Fe/Ni-N-C) were prepared by simple pyrolysis. The accelerants contain bimetallic Ni/Fe nanoparticles, $FeNi_3$ alloys, and compounds (Fe_2O_3, FeN, and Fe_3O_4). These components exhibit a high degree of graphitization, high pyridine-N and pyrrole-N contents, good stacking and wrinkled structures, and $Ni-N_x$ or $Fe-N_x$ active sites, resulting in enhanced electron transfer. The digesters with accelerants increased cumulative biogas production (402.95-587.76 mL/g VS) and TCOD degradation rates (36.39%-65.38%). The digestate of hybrid accelerants exhibited remarkable thermal stability (22.97%-32.75%) and fertility (4.43%-4.61%). The designed hybrid accelerants exhibited superior EEC (1.05-1.09 μmol e⁻/g). The enhanced methanogenesis in AcoD systems is attributable to the synergistic effects of different components (Fe and Ni metal nanoparticles, nitrides, oxides, and nitrogen-doped carbon) of hybrid accelerants.

DECLARATIONS

Authors' contributions

Investigation, formal analysis, data curation, writing-original draft: Ke T
Conceptualization, supervision, methodology, resources, visualization, funding acquisition, project administration, writing-review & editing: Yun S
Methodology, formal analysis: Wang K, Xing T, Dang J, Zhang Y, Sun M
Methodology: An J, Liu L, Liu J

Conflicts of interest
All authors declared that there are no conflicts of interest.

Ethical approval and consent to participate
Not applicable.

Consent for publication
Not applicable.

REFERENCES

1. Wang K, Yun S, Ke T, et al. Use of bag-filter gas dust in anaerobic digestion of cattle manure for boosting the methane yield and digestate utilization. *Bioresour Technol* 2022;348:126729. DOI
2. Huang X, Yun S, Zhu J, Du T, Zhang C, Li X. Mesophilic anaerobic co-digestion of aloe peel waste with dairy manure in the batch digester: focusing on mixing ratios and digestate stability. *Bioresour Technol* 2016;218:62-8. DOI
3. Ke T, Yun S, Wang K, An J, Liu L, Liu J. Enhanced anaerobic co-digestion performance by using surface-annealed titanium spheres at different atmospheres. *Bioresour Technol* 2022;347:126341. DOI
4. Li B, Yun S, Xing T, Wang K, Ke T, An J. A strategy for understanding the enhanced anaerobic co-digestion via dual-heteroatom doped bio-based carbon and its functional groups. *Chem Eng J* 2021;425:130473. DOI
5. Xu H, Yun S, Wang C, et al. Improving performance and phosphorus content of anaerobic co-digestion of dairy manure with aloe peel waste using vermiculite. *Bioresour Technol* 2020;301:122753. DOI
6. Jia B, Yun S, Shi J, et al. Enhanced anaerobic mono- and co-digestion under mesophilic condition: Focusing on the magnetic field and Ti-sphere core-shell structured additives. *Bioresour Technol* 2020;310:123450. DOI
7. Wu Y, Wang S, Liang D, Li N. Conductive materials in anaerobic digestion: from mechanism to application. *Bioresour Technol* 2020;298:122403. DOI
8. An J, Yun S, Wang W, et al. Enhanced methane production in anaerobic co-digestion systems with modified black phosphorus. *Bioresour Technol* 2023;368:128311. DOI
9. Xing T, Yun S, Li B, et al. Coconut-shell-derived bio-based carbon enhanced microbial electrolysis cells for upgrading anaerobic co-digestion of cow manure and aloe peel waste. *Bioresour Technol* 2021;338:125520. DOI
10. Li X, Yun S, Zhang C, Fang W, Huang X, Du T. Application of nano-scale transition metal carbides as accelerants in anaerobic digestion. *Int J Hydrog Energy* 2018;43:1926-36. DOI
11. Zhang T, Yun S, Li X, et al. Fabrication of niobium-based oxides/oxynitrides/nitrides and their applications in dye-sensitized solar cells and anaerobic digestion. *J Power Sources* 2017;340:325-36. DOI
12. Córdova-lizama A, Carrera-figueiras C, Palacios A, Castro-olivera P, Ruiz-espinoza J. Improving hydrogen production from the anaerobic digestion of waste activated sludge: effects of cobalt and iron zero valent nanoparticles. *Int J Hydrog Energy* 2022;47:30074-84. DOI
13. Abdelsalam E, Samer M, Attia Y, Abdel-hadi M, Hassan H, Badr Y. Influence of zero valent iron nanoparticles and magnetic iron oxide nanoparticles on biogas and methane production from anaerobic digestion of manure. *Energy* 2017;120:842-53. DOI
14. Zhang W, Zhang L, Li A. Enhanced anaerobic digestion of food waste by trace metal elements supplementation and reduced metals dosage by green chelating agent [S, S]-EDDS via improving metals bioavailability. *Water Res* 2015;84:266-77. DOI
15. Huang W, Yang F, Huang W, Wang D, Lei Z, Zhang Z. Weak magnetic field significantly enhances methane production from a digester supplemented with zero valent iron. *Bioresour Technol* 2019;282:202-10. DOI

16. Cubero-Cardoso J, Maluf Braga AF, Trujillo-Reyes Á, et al. Effect of metals on mesophilic anaerobic digestion of strawberry extrudate in batch mode. *J Environ Manag* 2023;326:116783. DOI

17. Abbas Y, Yun S, Wang Z, Zhang Y, Zhang X, Wang K. Recent advances in bio-based carbon materials for anaerobic digestion: a review. *Renew Sustain Energy Reviews* 2021;135:110378. DOI

18. Chen S, Rotaru AE, Shrestha PM, et al. Promoting interspecies electron transfer with biochar. *Sci Rep* 2014;4:5019. DOI PubMed PMC

19. Wang G, Li Q, Gao X, Wang XC. Synergetic promotion of syntrophic methane production from anaerobic digestion of complex organic wastes by biochar: performance and associated mechanisms. *Bioresour Technol* 2018;250:812-20. DOI

20. Wang J, Zhao Z, Zhang Y. Enhancing anaerobic digestion of kitchen wastes with biochar: Link between different properties and critical mechanisms of promoting interspecies electron transfer. *Renew Energy* 2021;167:791-9. DOI

21. Chen M, Shao L, Lv X, et al. In situ growth of Ni-encapsulated and N-doped carbon nanotubes on N-doped ordered mesoporous carbon for high-efficiency triiodide reduction in dye-sensitized solar cells. *Chem Eng J* 2020;390:124633. DOI

22. Dai Y, Chan Y, Jiang B, et al. Bifunctional Ag/Fe/N/C catalysts for enhancing oxygen reduction via cathodic biofilm inhibition in microbial fuel cells. *ACS Appl Mater Interfaces* 2016;8:6992-7002. DOI

23. Lai Y, Wang Q, Wang M, Li J, Fang J, Zhang Z. Facile synthesis of mesoporous Fe-N-C electrocatalyst for high performance alkaline aluminum-air battery. *J Electroanal Chem* 2017;801:72-6. DOI

24. Lu Z, Liu B, Dai W, Ouyang L, Ye J. Carbon network framework derived iron-nitrogen co-doped carbon nanotubes for enhanced oxygen reduction reaction through metal salt-assisted polymer blowing strategy. *Appl Surf Sci* 2019;463:767-74. DOI

25. Yun S, Zhang Y, Zhang L, Liu Z, Deng Y. Ni and Fe nanoparticles, alloy and Ni/Fe-N_x coordination co-boost the catalytic activity of the carbon-based catalyst for triiodide reduction and hydrogen evolution reaction. *J Colloid Interface Sci* 2022;615:501-16. DOI

26. Pei X, Peng X, Jia X, Wong PK. N-doped biochar from sewage sludge for catalytic peroxydisulfate activation toward sulfadiazine: efficiency, mechanism, and stability. *J Hazard Mater* 2021;419:126446. DOI PubMed

27. Abbas Y, Yun S, Mehmood A, et al. Co-digestion of cow manure and food waste for biogas enhancement and nutrients revival in bio-circular economy. *Chemosphere* 2023;311:137018. DOI

28. Abbas Y, Yun S, Wang K, Ali Shah F, Xing T, Li B. Static-magnetic-field coupled with fly-ash accelerant: a powerful strategy to significantly enhance the mesophilic anaerobic-co-digestion. *Bioresour Technol* 2021;327:124793. DOI

29. Wang Z, Yun S, Xu H, et al. Mesophilic anaerobic co-digestion of acorn slag waste with dairy manure in a batch digester: focusing on mixing ratios and bio-based carbon accelerants. *Bioresour Technol* 2019;286:121394. DOI

30. Yun S, Fang W, Du T, et al. Use of bio-based carbon materials for improving biogas yield and digestate stability. *Energy* 2018;164:898-909. DOI

31. Xu L, Fu B, Sun Y, et al. Degradation of organic pollutants by Fe/N co-doped biochar via peroxymonosulfate activation: synthesis, performance, mechanism and its potential for practical application. *Chem Eng J* 2020;400:125870. DOI

32. Li X, Jia Y, Zhou M, Su X, Sun J. High-efficiency degradation of organic pollutants with Fe, N co-doped biochar catalysts via persulfate activation. *J Hazard Mater* 2020;397:122764. DOI

33. Li L, Liu H, Chen Y, et al. Effect of magnet-Fe_3O_4 composite structure on methane production during anaerobic sludge digestion: establishment of direct interspecies electron transfer. *Renew Energy* 2022;188:52-60. DOI

34. Li S, Cao Y, Zhao Z, Zhang Y. Regulating secretion of extracellular polymeric substances through dosing magnetite and zerovalent iron nanoparticles to affect anaerobic digestion mode. *ACS Sustain Chem Eng* 2019;7:9655-62. DOI

35. Wang T, Zhang D, Dai L, Dong B, Dai X. Magnetite triggering enhanced direct interspecies electron transfer: a scavenger for the blockage of electron transfer in anaerobic digestion of high-solids sewage sludge. *Environ Sci Technol* 2018;52:7160-9. DOI

36. Yang L, Chen J, Park S, Wang H. Recent progress on metal-organic framework derived carbon and their composites as anode materials for potassium-ion batteries. *Energy Mater* 2023;3:300042. DOI

37. Wang Z, Yun S, Shi J, et al. Critical evidence for direct interspecies electron transfer with tungsten-based accelerants: an experimental and theoretical investigation. *Bioresour Technol* 2020;311:123519. DOI

38. Zhao J, Bao J, Yang S, et al. Exsolution-dissolution of supported metals on high-entropy $Co_3MnNiCuZnO_x$: toward sintering-resistant catalysis. *ACS Catal* 2021;11:12247-57. DOI

39. Zhang C, Yun S, Li X, Wang Z, Xu H, Du T. Low-cost composited accelerants for anaerobic digestion of dairy manure: focusing on methane yield, digestate utilization and energy evaluation. *Bioresour Technol* 2018;263:517-24. DOI

40. Liang S, Guo F, Du S, et al. Synthesis of Sargassum char-supported Ni-Fe nanoparticles and its application in tar cracking during biomass pyrolysis. *Fuel* 2020;275:117923. DOI

41. Xu L, Wu C, Liu P, et al. Peroxymonosulfate activation by nitrogen-doped biochar from sawdust for the efficient degradation of organic pollutants. *Chem Eng J* 2020;387:124065. DOI

42. Chen Y, Gokhale R, Serov A, Artyushkova K, Atanassov P. Novel highly active and selective Fe-N-C oxygen reduction electrocatalysts derived from in-situ polymerization pyrolysis. *Nano Energy* 2017;38:201-9. DOI

43. Yang C, Yun S, Shi J, et al. Tailoring the supercapacitive behaviors of Co/Zn-ZIF derived nanoporous carbon via incorporating transition metal species: a hybrid experimental-computational exploration. *Chem Eng J* 2021;419:129636. DOI

44. Zhang Y, Yun S, Sun M, et al. Implanted metal-nitrogen active sites enhance the electrocatalytic activity of zeolitic imidazolate zinc framework-derived porous carbon for the hydrogen evolution reaction in acidic and alkaline media. *J Colloid Interface Sci* 2021;604:441-57. DOI

45.　Chen X, Qin R, Li Z, Shan S, Liu Y, Yang C. One-pot synthesis of Fe/Cu/N-doped carbon materials derived from shale oil for efficient oxygen reduction reaction. *Mol Catal* 2021;500:111330. DOI

46.　Sun M, Yun S, Shi J, et al. Designing and understanding the outstanding tri-iodide reduction of N-coordinated magnetic metal modified defect-rich carbon dodecahedrons in photovoltaics. *Small* 2021;17:e2102300. DOI

47.　Cai H, Fu L, Pan H, Yan Z, Chen T, Zhao T. Pore engineering of ultramicroporous carbon from an N-doped polymer for CO_2 adsorption and conversion. *Mol Catal* 2023;550:113557. DOI

48.　Cheng H, Ji R, Bian Y, Jiang X, Song Y. From macroalgae to porous graphitized nitrogen-doped biochars - using aquatic biota to treat polycyclic aromatic hydrocarbons-contaminated water. *Bioresour Technol* 2020;303:122947. DOI PubMed

49.　Choi CH, Park SH, Woo SI. N-doped carbon prepared by pyrolysis of dicyandiamide with various $MeCl_2 \cdot xH_2O$ (Me = Co, Fe, and Ni) composites: effect of type and amount of metal seed on oxygen reduction reactions. *Appl Catal B Environ* 2012;119-20:123-31. DOI

50.　Luo B, Zhou L, Tian Z, He Y, Shu R. Hydrogenolysis of cornstalk lignin in supercritical ethanol over N-doped micro-mesoporous biochar supported Ru catalyst. *Fuel Process Technol* 2022;231:107218. DOI

51.　Wang X, Yun S, Zhang Y, et al. Boosting catalytic activity of niobium/tantalum-nitrogen active-sites for triiodide reduction in photovoltaics. *J Colloid Interface Sci* 2021;603:651-65. DOI

52.　Huang Z, Zhou H, Yang W, Fu C, Chen L, Kuang Y. Three-dimensional hierarchical porous nitrogen and sulfur-codoped graphene nanosheets for oxygen reduction in both alkaline and acidic media. *ChemCatChem* 2017;9:987-96. DOI

53.　Chan Y, Dai Y, Li R, Zou J, Tian G, Fu H. Low-temperature synthesized nitrogen-doped iron/iron carbide/partly-graphitized carbon as stable cathode catalysts for enhancing bioelectricity generation. *Carbon* 2015;89:8-19. DOI

54.　Masa J, Sinev I, Mistry H, et al. Ultrathin high surface area nickel boride (Ni_xB) nanosheets as highly efficient electrocatalyst for oxygen evolution. *Adv Energy Mater* 2017;7:1700381. DOI

55.　Chen B, Wang D, Zhang B, et al. Engineering the active sites of graphene catalyst: from CO_2 activation to activate Li-CO_2 batteries. *ACS Nano* 2021;15:9841-50. DOI

56.　Xiong Y, Li H, Liu C, et al. Single-atom Fe catalysts for fenton-like reactions: roles of different N species. *Adv Mater* 2022;34:e2110653. DOI

57.　Zhou Y, Li Y, Zhang L, et al. Fe-leaching induced surface reconstruction of Ni-Fe alloy on N-doped carbon to boost oxygen evolution reaction. *Chem Eng J* 2020;394:124977. DOI

58.　Deng Y, Yun S, Dang J, et al. A multi-dimensional hierarchical strategy building melamine sponge-derived tetrapod carbon supported cobalt-nickel tellurides 0D/3D nanohybrids for boosting hydrogen evolution and triiodide reduction reaction. *J Colloid Interface Sci* 2022;624:650-69. DOI

59.　Dang J, Yun S, Zhang Y, et al. Constructing double-shell structured N-C-in-Co/N-C electrocatalysts with nanorod- and rhombic dodecahedron-shaped hollow morphologies to boost electrocatalytic activity for hydrogen evolution and triiodide reduction reaction. *Chem Eng J* 2022;449:137854. DOI

60.　Shen Y, Linville JL, Urgun-demirtas M, Schoene RP, Snyder SW. Producing pipeline-quality biomethane via anaerobic digestion of sludge amended with corn stover biochar with in-situ CO_2 removal. *Appl Energy* 2015;158:300-9. DOI

61.　Han F, Yun S, Zhang C, Xu H, Wang Z. Steel slag as accelerant in anaerobic digestion for nonhazardous treatment and digestate fertilizer utilization. *Bioresour Technol* 2019;282:331-8. DOI

62.　Liu L, Yun S, Ke T, Wang K, An J, Liu J. Dual utilization of aloe peel: aloe peel-derived carbon quantum dots enhanced anaerobic co-digestion of aloe peel. *Waste Manag* 2023;159:163-73. DOI

63.　Yun S, Xing T, Wang Y, et al. Mineral residue accelerant-enhanced anaerobic digestion of cow manure: an evaluation system of comprehensive performance. *Sci Total Environ* 2023;858:159840. DOI

64.　Yun S, Xing T, Han F, et al. Enhanced direct interspecies electron transfer with transition metal oxide accelerants in anaerobic digestion. *Bioresour Technol* 2021;320:124294. DOI

65.　Zhang W, Lang Q, Wu S, Li W, Bah H, Dong R. Anaerobic digestion characteristics of pig manures depending on various growth stages and initial substrate concentrations in a scaled pig farm in Southern China. *Bioresour Technol* 2014;156:63-9. DOI

66.　Xie S, Wickham R, Nghiem LD. Synergistic effect from anaerobic co-digestion of sewage sludge and organic wastes. *Int Biodeter Biodegr* 2017;116:191-7. DOI

67.　Kumar A, Singh E, Singh L, Kumar S, Kumar R. Carbon material as a sustainable alternative towards boosting properties of urban soil and foster plant growth. *Sci Total Environ* 2021;751:141659. DOI

68.　Zhang A, Bian R, Pan G, et al. Effects of biochar amendment on soil quality, crop yield and greenhouse gas emission in a Chinese rice paddy: a field study of 2 consecutive rice growing cycles. *Field Crops Res* 2012;127:153-60. DOI

69.　Li Y, Chen Y, Wu J. Enhancement of methane production in anaerobic digestion process: a review. *Appl Energy* 2019;240:120-37. DOI

70.　Lovley DR. Syntrophy goes electric: direct interspecies electron transfer. *Ann Rev Microbiol* 2017;71:643-64. DOI

71.　Yang Y, Zhang Y, Li Z, Zhao Z, Quan X, Zhao Z. Adding granular activated carbon into anaerobic sludge digestion to promote methane production and sludge decomposition. *J Clean Prod* 2017;149:1101-8. DOI

72.　Barua S, Dhar BR. Advances towards understanding and engineering direct interspecies electron transfer in anaerobic digestion. *Bioresour Technol* 2017;244:698-707. DOI PubMed

73.　Chen J, Yun S, Shi J, et al. Role of biomass-derived carbon-based composite accelerants in enhanced anaerobic digestion: focusing on biogas yield, fertilizer utilization, and density functional theory calculations. *Bioresour Technol* 2020;307:123204. DOI

74. Liang M, Liu Y, Zhang J, et al. Understanding the role of metal and N species in M@NC catalysts for electrochemical CO_2 reduction reaction. *Appl Catal B Environ* 2022;306:121115. DOI
75. Wang J, Zhu W, Meng F, Bai G, Zhang Q, Lan X. Integrating dual-metal sites into covalent organic frameworks for enhanced photocatalytic CO_2 reduction. *ACS Catal* 2023;13:4316-29. DOI
76. Ran L, Li Z, Ran B, et al. Engineering single-atom active sites on covalent organic frameworks for boosting CO_2 photoreduction. *J Am Chem Soc* 2022;144:17097-109. DOI